

Macrobubble clouds produced by breaking wind waves: A laboratory study

Peter M. Kalvoda,¹ Lilun Xu,² and Jin Wu³

Air-Sea Interaction Laboratory, Graduate College of Marine Studies, University of Delaware, Lewes, Delaware, USA

Received 23 April 1998; revised 21 February 2003; accepted 8 April 2003; published 28 June 2003.

[1] Clouds of large air bubbles produced by breaking wind waves have been studied in a laboratory tank. Temporal evolutions of these macrobubble clouds, including their length scales, aspect ratios, area scales, and velocities, are presented; the bubble concentration and void ratio within the cloud are also found. The initial downwind velocity of the cloud is about one half, but can reach about two thirds, the phase velocity of the breaking wave. The maximum penetrating depth of the cloud is about one half the breaking wave height. All these geometric and kinematic characteristics of the cloud are also associated with those of the breaking wave. *INDEX TERMS:* 4504 Oceanography: Physical: Air/sea interactions (0312); 4560 Oceanography: Physical: Surface waves and tides (1255); 4572 Oceanography: Physical: Upper ocean processes

Citation: Kalvoda, P. M., L. Xu, and J. Wu, Macrobubble clouds produced by breaking wind waves: A laboratory study, *J. Geophys. Res.*, 108(C6), 3207, doi:10.1029/1999JC000265, 2003.

1. Introduction

[2] Air bubbles in the near-surface ocean influence many important oceanographic phenomena such as the attenuation of underwater sound [Novarini *et al.*, 1998], the generation of oceanic noise [Updegraff and Anderson, 1991], the air-sea exchange of heat and mass [Andreas and Monahan, 2000], and the production of marine aerosols [Wu, 2000]. Bubbles in the field were measured by Blanchard and Woodcock [1957], Kolovayev [1976], Johnson and Cooke [1979], Thorpe [1982, 1986], and Medwin and Breitz [1989]. On the basis of their results, parametric descriptions were developed of bubble characteristics in the near-surface ocean [Wu, 1994]. Experiments were also conducted in wind-wave tanks [Koga, 1982; Baldy and Bourguel, 1987; Baldy, 1988; Hwang *et al.*, 1990], while a theoretical model of ambient and transient bubbles was presented by Baldy [1993].

[3] Bubbles are produced through air becoming entrained by breaking waves. Large bubbles freshly generated below the breaker are in a plume-like structure [Koga, 1982]; these macrobubbles soon return to the sea surface and burst. Small bubbles are suspended and dispersed in a shallow interface layer immediately below the undulating sea surface [Wu, 1994]. Lamarre and Melville [1992, 1994] measured the void fraction in the bubble cloud produced by plunging breakers in a wave tank; their results also included the temporal variation of horizontal and vertical centroids of the cloud.

[4] Experiments were performed on macrobubble clouds produced by breaking wind waves in the Wind-Wave-Current Research Facility of the University of Delaware, Lewes, Delaware. The temporal evolution of clouds, including their occurrence, growth, and decay, was observed. The maximum penetrating depth of the cloud was found to be one half the wave height. The maximum cloud area is about $HL/3$, where H and L are the height and the length of breaking waves, respectively. The lifetime of the macrobubble cloud is ~ 1.4 times the wave period. Sizes of bubbles in the cloud on the large diameter side follow a distribution of d^{-2} for $d < 5$ mm and of $d^{-3.7}$ for larger bubbles, where d is the bubble diameter.

2. Experiments

2.1. Facility and Experimental Conditions

[5] The experiment was conducted in the Wind-Wave-Current Research Facility; it is 37 m long, 1 m wide, and 1.3 m high. The facility was filled with fresh water to a depth of 76 cm. Air and water temperatures within the facility were both at 18°C. Waves were generated by a forced air system, which is capable of providing a maximum wind velocity of 18 m s⁻¹. Waves were absorbed by a 1-in-10-slope beach at the end of the tank. Measurements were conducted at a fetch of 16 m, which was sufficiently far from the downwind end of the tank to avoid the influence of the beach. Measurements were performed at the wind velocity of 16 m s⁻¹. At this velocity, every dominant wave broke, while at higher velocities, spray droplets made visual observations through the transparent sidewalls of the tank impossible.

2.2. Observations of the Macrobubble Cloud

2.2.1. Observation Procedure

[6] A video camera (Panasonic AG-160), a Canon camera (T90 35 mm), and an image analysis system (EPIX Model

¹Now at Visteon Corporation, Dearborn, Michigan, USA.

²Now at Ocean University of Qingdao, Qingdao, Shandong, China.

³Now at Institute of Hydraulic and Ocean Engineering, National Cheng Kung University, Tainan, Taiwan.

4MIP) were grouped to provide the data acquisition and analysis. The video camera operated at 30 frames s^{-1} ; its high-speed shutter produced exposures of $1/1000 \text{ s}$ during each frame. The bubble cloud was first traced; subsequently, its boundary was digitized with the image analysis system in order to display it on a color video monitor for further processing. The displacement observed between frames could be converted to the rate of change over integer multiples of $1/30 \text{ s}$. The total area within the cloud boundary was computed by the software provided.

[7] The video camera provided side and top views of the macrobubble cloud. Horizontal and vertical fields in the side view covered $0.79 \times 0.59 \text{ m}$, with the former being about three fourths the length of the breaking waves. The camera lens axis was aligned with the mean water surface and perpendicular to the sidewalls of the tank. Four 500-W quartz tungsten lamps were placed at the back side of the tank. A sheet of white translucent paper was used to diffuse the light over the illuminated area. Later, the video camera was placed on top of the tank looking downward over a surface area of $0.66 \times 0.5 \text{ m}$.

[8] The Canon camera also photographed macrobubble clouds from the side view. An analog timer was placed within the image field of both the Canon and the video camera. The video camera, having a much larger field of view than the Canon camera, was used to obtain the period and height of waves. The lengths and phase speeds of the breaking waves were approximately calculated by the linear wave theory from the wave period measured with the video camera.

[9] Bubble sizes were measured from photographs taken with the Canon camera. Some bubbles were elliptical; their major and minor axes, d_1 and d_2 , were obtained to determine the area of the ellipse calculated from $\pi d_1 d_2 / 4$. The equivalent diameter of a circle having the same area of the ellipse was then calculated: $d = (d_1 d_2)^{1/2}$.

2.2.2. Measurement Accuracies

[10] There are two basic uncertainties in measuring the macrobubble cloud with the video camera. These are associated with either various cloud locations along the camera axis or with the camera lens distortion. The maximum uncertainty in cloud spatial dimensions is the ill-defined camera-cloud location for the side and top views, estimated to be 26% and 8.2%, respectively. The maximum uncertainty due to the lens distortion is 6.3%, which is applicable to both top and side views. The combined underestimation of the cloud size for the side view could be 29%. However, for any clouds viewed from the side this underestimation would be constant since the cloud always translates in the direction of the wind-wave propagation. The total underestimation of the cloud size from the top view is much less, $\sim 14\%$. This field of view permits a calculated bubble resolution of 1 mm in diameter. Also, the manual positioning of the cursor of the image analysis system during spatial measurements imposes a precision limit.

[11] The height, length, and phase speed of waves were used as scaling parameters for macrobubble cloud data. The maximum error was estimated to be 5% for the wave period. This would result in an error of 10% for the wavelength and of 5% for the wave phase velocity. In addition, the resolution in the wave height was 5 mm for both the video camera and

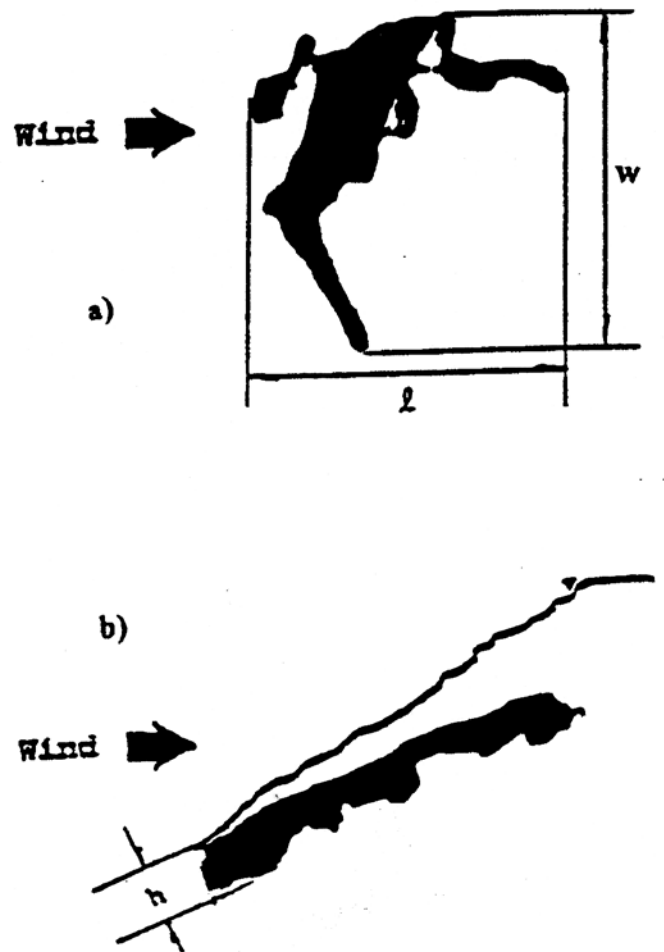


Figure 1. Definition sketch of the cloud: (a) top and (b) side views.

the image analysis system; it would lead to a maximum of 5% error for the smallest wave height, measured at $\sim 10 \text{ cm}$.

3. Results and Analyses

[12] The dimensions of a macrobubble cloud are defined in Figure 1; its top view is shown in Figure 1a, where w and l are the width and the length of the cloud, respectively. The wind direction is from left to right. The penetrating depth of the cloud, h , is defined in Figure 1b and is the maximum depth perpendicular to the local water surface. Five side and top views of waves and clouds were analyzed; images from these two views are shown as the shaded areas in Figures 2 and 3. In both figures, t is time (s), started at the inception of wave breaking.

3.1. Cloud Sequence

[13] The time interval between images of the macrobubble cloud shown in Figure 2 is $1/30 \text{ s}$. The top line in Figure 2 corresponds to the water surface at the sidewall of the tank; the middle line attached to the shaded area corresponds to the lower boundary of the water surface. Owing to the three-dimensional structure of waves, the water surface was wavy not only along but also across the tank. The region bounding the top and middle lines indicates that the water surface sloped down away from the

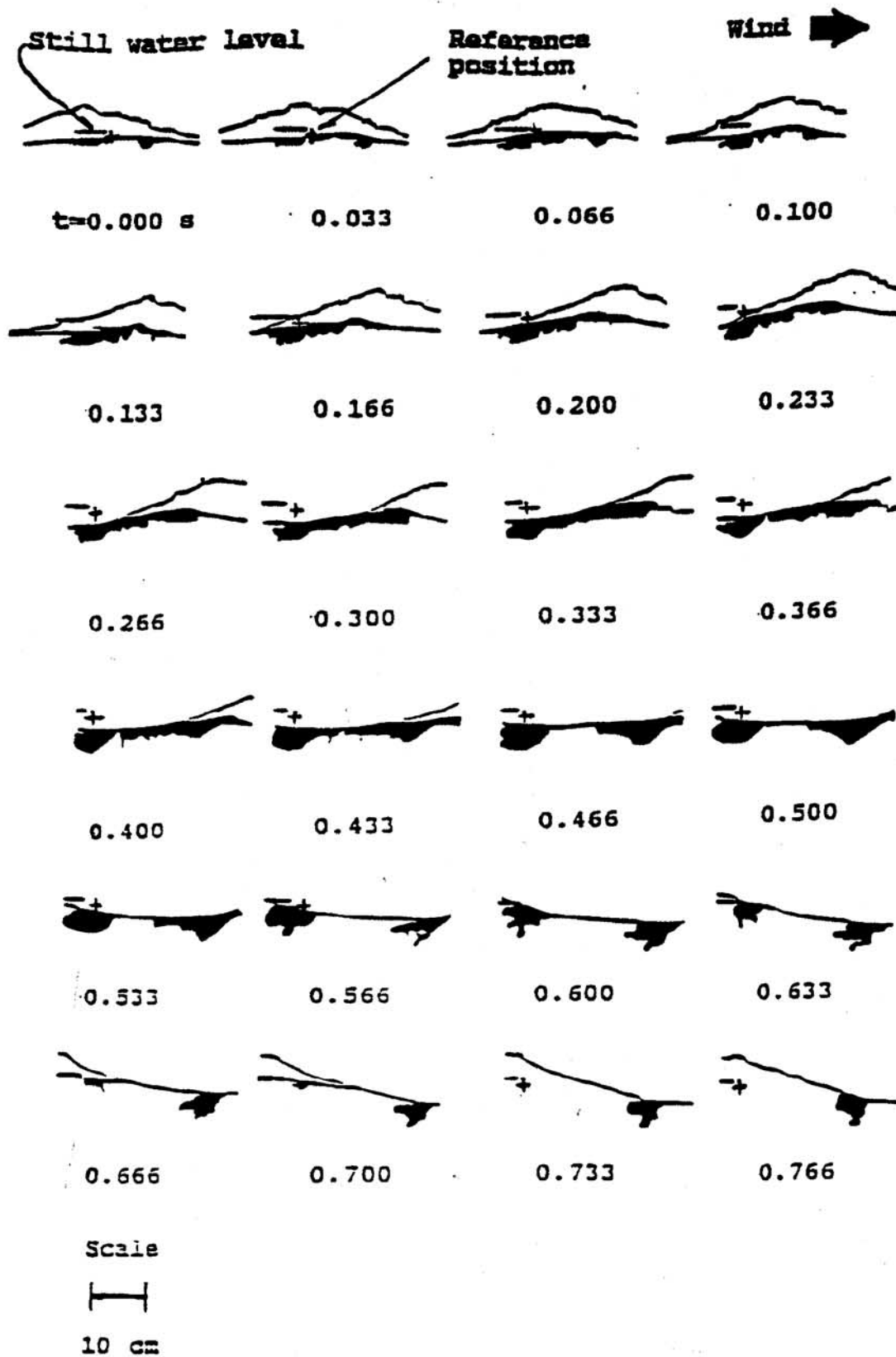


Figure 2. Time sequence of the macrobubble cloud (side view) with $T = 0.65$ s. The time runs from left to right and from top to bottom. The time interval is $1/30$ s.

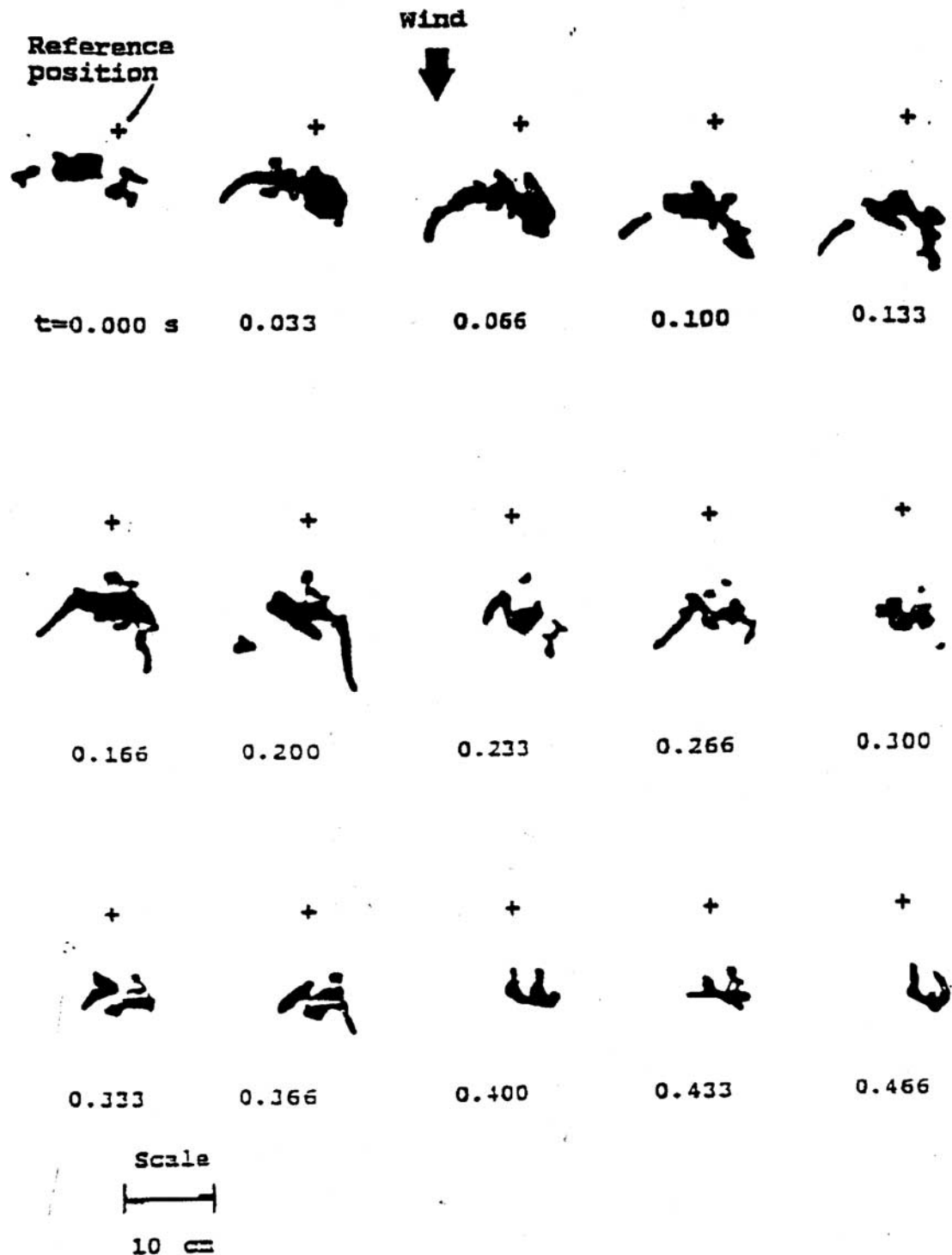


Figure 3. Same as 2, but for the top view.

sidewall. This region is the underside view of the wave. The latter scattered the light, making observations of the bubble cloud impossible in this region. There were no bubble clouds before the first image shown.

[14] In presenting our results, the time was normalized with the period of breaking waves, T . Images before $t/T = 0.5$ correspond to cloud growth, where the cloud length and penetration depth increase. The image at $t/T = 0.5$ is defined as the fully developed cloud, where the total contiguous area

reaches a maximum value. At $t/T = 0.56$ the cloud starts to decay by breaking up into two discrete portions; from then on the length of these two distinct portions becomes foreshortened. One portion still exists at the time of $1.4T$ without the presence of the next breaking wave; it is not plotted here. The penetration depth is seen in Figure 2 to continuously increase from the beginning of wave breaking.

[15] Figure 3 shows the top view sequence before $t/T = 0.72$. The cloud appears irregularly shaped. The length to

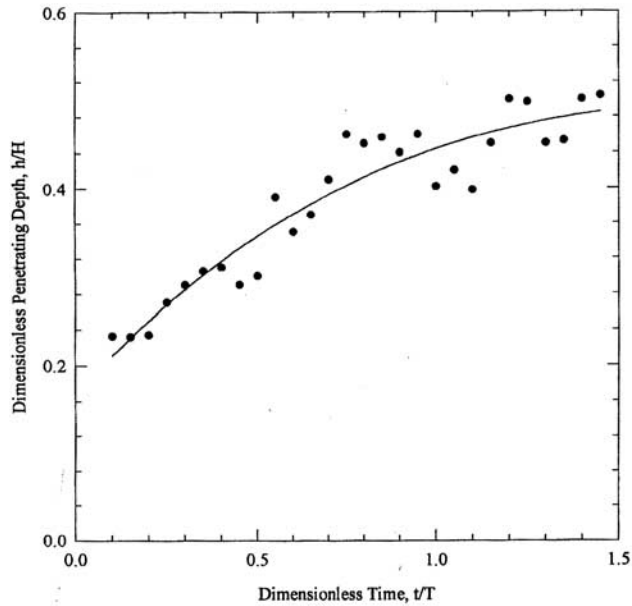


Figure 4. Penetrating depth of the cloud versus time (side view).

width ratio of the cloud is approximately the same throughout its lifetime. The maximum area of the cloud occurs at $t/T = 0.25$ and then decreases. The cloud from the top view spreads faster at the water surface, whereas the cloud from the side view later spreads to its maximum area $0.25T$ after reaching its maximum area from the top view. This happens because it is necessary for bubbles at the water surface to have enough time to penetrate more deeply.

3.2. Cloud Length Scales

[16] In the following, data are presented of mean values for five sets of side and top views; the maximum standard deviation of data from the mean value is $<28\%$.

[17] Figure 4 shows dimensionless penetration depth, h/H , at the side view. Bubbles are continuously dispersed to a deeper depth due to the turbulent diffusion. The penetration depth gradually increases before $t/T \approx 0.6$. Subsequently, the cloud breaks up, and soon, one of the discrete clouds goes to the water surface; the other is stretched and forced to move downward up to $t/T \approx 1.4$. It is seen in Figure 4 that the maximum penetration depth of the cloud is about one half the wave height below the water surface.

[18] The solid line in Figure 5 represents the dimensionless side view of l/L data. Up to $t/T \approx 0.2$ the cloud length increases rapidly, reaching its maximum value of 0.16 at $t/T \approx 0.4$. Subsequently, the cloud length decreases. The dashed line in Figure 5 represents the same kind of dimensionless data of l/L versus t/T for the top view, with the cloud length being $\sim 0.1L$ for the duration of measurements. The relative constancy of the cloud length viewed from the top indicates a continuous return of bubbles to the water surface. Variations in t/T of the dimensionless width, w/L , at the top view, not shown here, follow a similar pattern.

3.3. Cloud Aspect Ratios

[19] Figure 6 is a plot of the aspect ratio h/l . Following the occurrence of breaking, the value of h/l decreases down

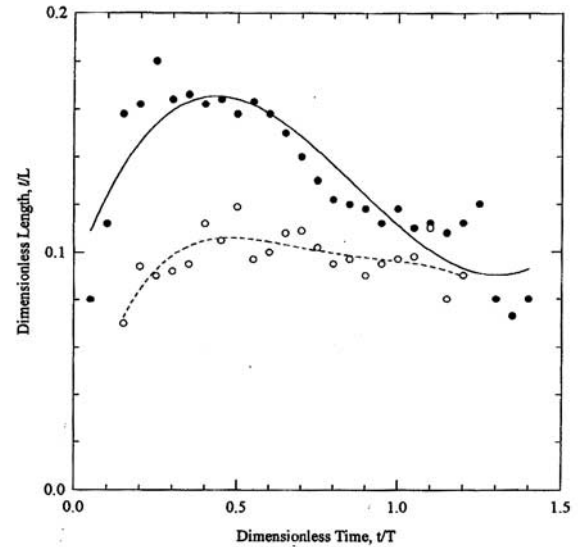


Figure 5. Cloud length versus time. The solid curve and solid symbols are for the side view, and the dashed curve and open symbols are for the top view.

to $t/T \approx 0.2$. In this initial period the value of h is almost unchanged, whereas the length of the cloud, l , does develop longer. In the time period of $t/T \approx 0.2-0.6$ the ratio h/l continuously increases because h increases and l remains nearly unchanged. After $t/T \approx 0.6$, l is reduced, so h/l is still enhanced. The aspect ratio l/w , as viewed from the top, is approximately unity over the lifetime of the cloud (not shown). In addition, breaking often occurs at more than one localized point near the wave crest. These waves are generally three-dimensional.

3.4. Cloud Area Scales

[20] The solid line in Figure 7 shows a plot of the dimensionless cloud area A/HL from the side view. The

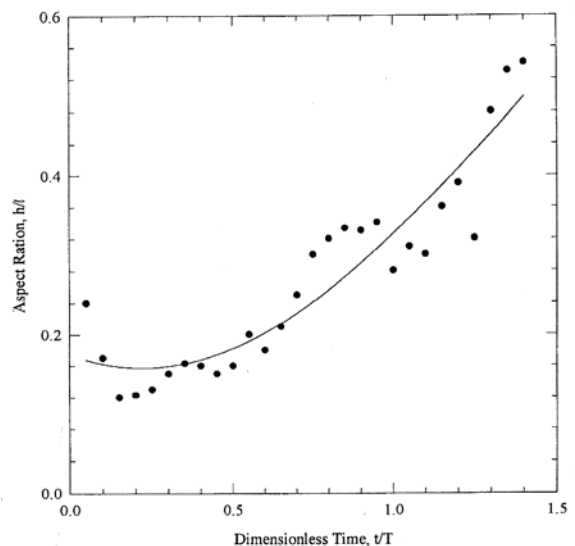


Figure 6. Aspect ratio of the cloud versus time (side view).

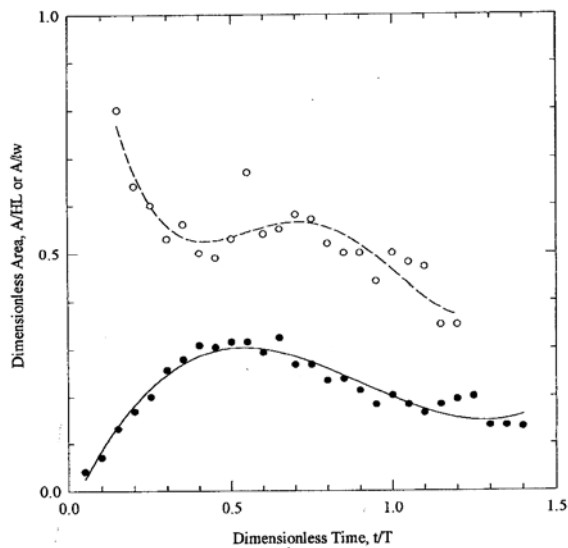


Figure 7. Cloud area versus time. The solid curve and solid symbols are for dimensionless cloud area A/HL at the side view, and the dashed curve and open symbols are for dimensionless cloud area A/lw at the top view.

wave height determines the maximum vertical entrainment of bubbles, while the length of freshly produced cloud varies with the length of the breaking waves. Therefore the cloud area can be scaled with the product of the above two parameters, H and L .

[21] The maximum cloud area, $A/HL \approx 0.33$, is shown to occur at $t/T \approx 0.5$, which corresponds to the time at the wave trough. Initially, the rate of area growth increases up to $t/T \approx 0.35$ and is proportional to $0.8cH$, where c is the phase velocity of the parent breaking wave; it then levels off to about zero up to $t/T \approx 0.5$. Thereafter the growth rate becomes negative; its magnitude, however, is not as great as it was during the first one third of the wave period. This is reasonable in that the cloud decays due to the return of bubbles to the water surface, which is governed by the buoyant force.

[22] The dashed line in Figure 7 shows the evolution of dimensionless area A/lw , obtained from measurements of the top view. The value of A/lw reaches its maximum before $t/T \approx 0.3$. The reason is that bubbles in the cloud at the beginning of breaking are packed together to make l and w shorter. After $t/T \approx 0.3$, bubbles spread to make both l and w greater; the value of A/lw , therefore, has a tendency to decrease with time. It essentially shows that the total area of cloud is about one half the product of the length and width of the cloud.

3.5. Cloud Velocity

[23] Figure 8 shows the dimensionless horizontal edge position of the cloud normalized by the wavelength, X/L , at the side view. The slope of the inclined lines represents the ratio of the downwind velocity of the cloud to the phase velocity of the breaking wave:

$$V_h = \alpha_1 c,$$

where V_k is the downwind velocity. The time variation of α_1 is shown as the solid symbols in Figure 9. The initial

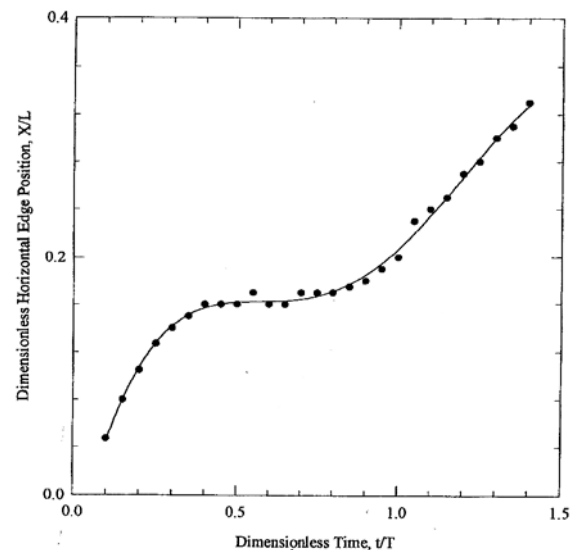


Figure 8. Horizontal edge position versus time (side view).

downwind velocity is seen in Figure 9 to be $\sim 0.66c$ at $t/T = 0.1$. The average downwind velocity of the cloud is $\sim 0.45c$ up to $t/T \approx 0.1$ and approaches zero up to $t/T \approx 0.7$. The cloud velocity then increases again to reach $\sim 0.3c$ at $t/T \approx 1.4$. The velocity of $0.45c$ corresponds approximately to the maximum value of the wave orbital velocity for an ideal sinusoidal wave. This is consistent with the observation that whitecaps move downwind at a velocity which is typically one half the phase velocity of the breaking waves [Snyder *et al.*, 1983; Hwang *et al.*, 1990]. The cloud velocity is near zero at the wave trough ($0.4 < t/T < 0.7$), where the whitecap velocity is equal, but opposite, to that of the horizontal water particle velocity. The increase in the cloud velocity during the later stage for $t/T > 0.9$ is due to the arrival of another

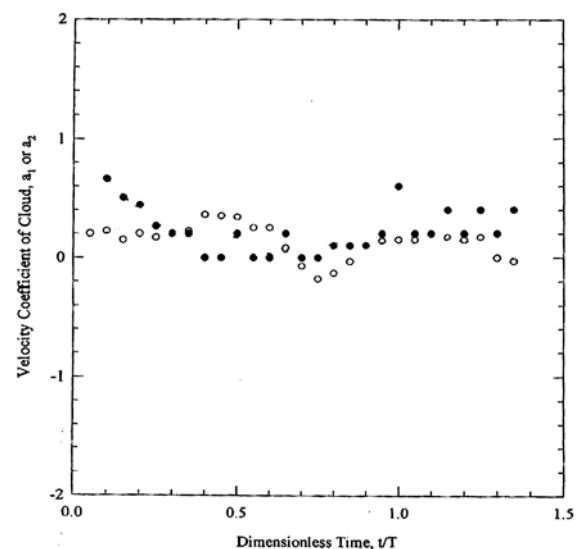


Figure 9. Velocity coefficient of the cloud versus time at the side view. The solid symbols are for the horizontal velocity, and the open symbols are for the vertical velocity.

wave, which imparts momentum to the cloud. The variation of X/L versus t/T at the top view, not shown here, is essentially consistent with that shown in Figure 8.

[24] The penetration velocity of the cloud, V_p , can be denoted as

$$V_p = \alpha_2 H/T.$$

The time variation coefficient α_2 is plotted as the open symbols in Figure 9. The cloud continuously develops along the vertical direction before $t/T \approx 0.5$. At that time the penetration speed in the vertical direction is $\sim 0.3H/T$. Some bubbles go back to the water surface quickly and disappear in the cloud after $t/T \approx 0.5$. A few bubbles keep on going deeper, and the lifetime of these bubbles can reach $1.4T$.

3.6. Macrobubbles Within the Cloud

[25] The number and sizes of macrobubbles within five fully developed clouds were measured from the side view. Criterion defining the lower boundary was the resolution limit on the bubble size of ~ 1 mm, which was determined by measuring bubbles directly. Bubbles sufficiently distant from the bulk were not considered to be a part of the cloud. Some of the largest void areas are due to bubbles in contact with each other. Most bubbles observed were spherical, and some large bubbles were elliptic.

[26] The distribution of bubble sizes within fully developed macrobubble clouds is shown in Figure 10. The bubble concentration varies with the diameter over the whole range of measurements as

$$N(d) \sim d^{-3.2}, \quad 1\text{ mm} < d < 10\text{ mm}$$

where N is the bubble concentration per mm of diameter and the bubble concentration per cm^3 of water. It can be seen from Figure 10 that the data are divided into two groups. Bubbles smaller than 5 mm in diameter follow the size spectrum of

$$N(d) \sim d^{-2}, \quad 1\text{ mm} < d < 5\text{ mm}$$

while those larger than 5 mm in diameter follow

$$N(d) \sim d^{-3.7}, \quad 5\text{ mm} < d \leq 10\text{ mm}$$

3.7. Void Ratio

[27] The void ratio was obtained by summing the total volume of all bubbles in the cloud divided by the volume of the cloud. The latter was defined as wA ; $A \approx 0.33HL$ is the side view area of the fully developed cloud, and $w \approx 0.1L$ is the top view cloud width below the water surface. If the presence of large voids, which were in contact with the water surface, was neglected, the void ratio would be $\sim 0.4\%$ for two fully developed macrobubble clouds.

4. Comparison With Other Studies

4.1. Entrainment Depth

[28] The ratio of cloud entrainment depth to wave height is very similar to the ratio of cloud penetration depth to wave height; this ratio is found to be ~ 0.5 . It compares well

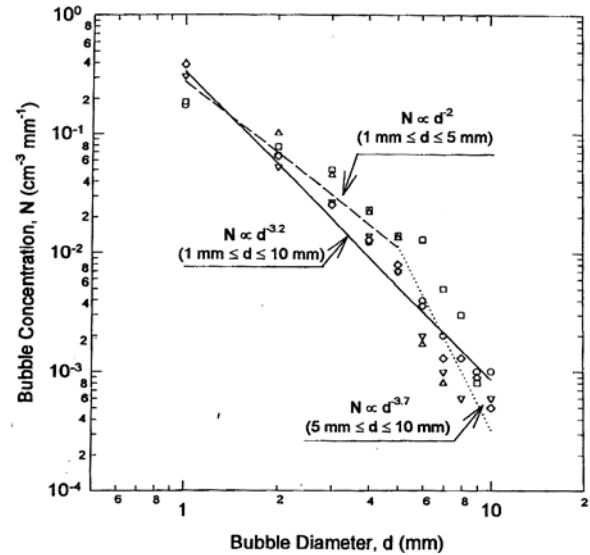


Figure 10. Bubble concentration versus bubble diameter of 1–10 mm within five fully developed macrobubble clouds. Their wave heights and periods are as follows: $H = 8.5$ cm, $T = 73$ s (diamonds); $H = 6.7$ cm, $T = 0.70$ s (circles); $H = 8.2$ cm, $T = 0.65$ s (triangles); $H = 7.4$ cm, $T = 0.67$ s (squares); and $H = 9.7$ cm, $T = 0.73$ s (inverted triangles).

with the entrainment depth reported by *Koga* [1982], who found bubbles from one half to one wave height away from the water surface. *Lamarre and Melville* [1991] also found that bubbles penetrated down to a depth of about one wave height with plunging breakers; the latter may have a larger entrainment depth than that for spilling breakers in the present study.

4.2. Bubble Size Distribution

[29] The size distribution of bubbles in our experiments follows d^{-2} for the diameter range of $1\text{ mm} < d \leq 5\text{ mm}$. This is comparable with $d^{-2.5}$ reported by *Medwin and Breitz* [1989] near the ocean surface; the largest diameter of bubbles in their experiment is $< 100\text{ }\mu\text{m}$. *Baldy* [1993] found theoretically that the concentration for transient bubbles follows d^{-2} in the close vicinity of breaking waves, including all bubbles $< 3\text{ mm}$ in diameter. The results and the bubble diameter range in our experiments are similar to those reported by *Baldy* [1993].

4.3. Cloud Aspect Ratio

[30] The ratio between the length (along the tank) and width (across the tank) of the cloud observed on the water surface was $\sim 1:1$. This contrasts with field observations of whitecaps reported by *Bortkovskii* [1987], who found that the ratio was $\sim 2:1$. This difference between the laboratory and field results is not unreasonable, as waves in the field have very long crests.

4.4. Cloud Velocity

[31] Analysis of measurements from the side and top views showed the average horizontal cloud velocity to be approximately half the wave phase velocity up to $t/T \approx 0.4$. This is similar to the results of *Snyder et al.* [1983].

[32] When the wave breaks, the horizontal water particle velocity exceeds the wave phase velocity. The process of breaking involves the formation of a spilling region ahead of the wave crest, which advances in pace with the wave crest. This is the velocity at the water surface; the current velocity, however, decreases away from being nearly the phase velocity at the beginning of wave breaking to a certain fraction of the phase velocity as bubbles penetrate more deeply. It is seen from Figure 9 that the horizontal velocity of the cloud is $\sim 0.66c$ at $t/T = 0.1$. Lamarre and Melville [1994] found that the initial horizontal velocity of the plume is $\sim 0.7c$. Our experimental result is similar.

[33] The vertical motion of the cloud measured is near $0.3H/T$ or $\sim 4 \text{ cm s}^{-1}$; this represents the velocity of bubbles being entrained into a deeper depth. Lamarre and Melville [1994] showed the magnitude of velocity to be $0.2H/T$ for the bubble plume in the wave tank, which approximates our measurements.

4.5. Void Ratio

[34] At $t/T = 0.4$ the void fraction of 0.4% was obtained in our experiment, while for the same dimensionless time, Lamarre and Melville [1991] reported a void fraction of up to 6%. Such a large difference is probably due to the fact that the breaking waves in their study were plunging breakers, but in the present study they were spilling breakers. Plunging breakers are known to enclose, and subsequently entrain, a much larger volume of air. In addition, their measurement volume was $\sim 90 \text{ cm}^3$ in comparison with 1600 and 2700 cm^3 in the present study. If a larger volume is taken, the void ratio in the outer edge of the volume is very small; it does not contribute much to the total volume of air. The largest bubble observed by Lamarre and Melville was 12 mm in diameter as compared with ~ 10 mm in the present study.

5. Summary and Conclusion

[35] The macrobubble cloud produced by breaking waves grows with time to reach the maximum area near the wave trough at the side view after the wave breaks, but the maximum area at the top view occurs at $0.25T$. After the time of $0.5T$ at the side view the cloud decays and divides into two discrete parts; most bubbles return to the surface soon, but a few bubbles still go deeper. The cloud at the top view is more irregular than the cloud at the side view; the lifetime at the top view is $0.7T$. The maximum penetration depth of the cloud under the water surface approaches half the wave height. The maximum cloud lengths at the top view and the side view are $0.1L$ and $0.16L$, respectively. The cloud width at the top view is $0.1L$. The average horizontal cloud speed can reach ~ 0.45 times the phase speed before the wave trough occurs. The void ratio in the macrobubble cloud is $\sim 0.4\%$. The bubble concentration in the cloud varies with diameter as $d^{-3.2}$ for bubbles with diameters from 1 to 10 mm.

[36] **Acknowledgments.** This article originated from the master's thesis of the first author (PMK). It was supported by the Office of Naval Research (ASSERT Program) through grant N00014-93-1-0727. Duncan C. Blanchard, who served on PMK's thesis committee, offered valuable help to this work.

References

- Andreas, E. L., and E. C. Monahan, The role of whitecap bubbles in air-sea heat and moisture exchange, *J. Phys. Oceanogr.*, *30*, 433–442, 2000.
- Baldy, S., Bubbles in the close vicinity of breaking waves: Statistical characteristics of the generation and dispersion mechanism, *J. Geophys. Res.*, *93*, 8239–8248, 1988.
- Baldy, S., A generation-dispersion model of ambient and transient bubbles in the close vicinity of breaking waves, *J. Geophys. Res.*, *98*, 18277–18293, 1993.
- Baldy, S., and M. Bourguel, Bubbles between the wave trough and wave crest levels, *J. Geophys. Res.*, *92*, 2919–2929, 1987.
- Blanchard, D. C., and A. H. Woodcock, Bubble formation and modification in the sea and its meteorological significance, *Tellus*, *9*, 145–158, 1957.
- Bortkovskii, R. S., *Air-Sea Exchange of Heat and Moisture During Storms*, 194 pp., D. Reidel, Norwell, Mass., 1987.
- Hwang, P. A., Y.-H. L. Hsu, and J. Wu, Air bubbles produced by breaking wind waves: A laboratory study, *J. Phys. Oceanogr.*, *20*, 19–28, 1990.
- Johnson, B. D., and R. C. Cooke, Bubble populations and spectra in coastal waters: A photographic approach, *J. Geophys. Res.*, *84*, 3761–3766, 1979.
- Koga, M., Bubble entrainment in breaking wind waves, *Tellus*, *34*, 481–489, 1982.
- Kolovayev, P. A., Investigation of the concentration and statistical size distribution of wind-produced bubbles in the near-surface ocean layer, *Oceanology, Engl. Transl.*, *15*, 659–661, 1976.
- Lamarre, E., and W. K. Melville, Air entrainment and dissipation in breaking waves, *Nature*, *351*, 469–472, 1991.
- Lamarre, E., and W. K. Melville, Instrumentation for the measurement of void-fraction in breaking waves: Laboratory and field results, *IEEE J. Oceanic Eng.*, *17*, 204–215, 1992.
- Lammare, E., and W. K. Melville, Void-fraction measurements and sound-speed fields in bubble plumes generated by breaking waves, *J. Acoust. Soc. Am.*, *93*, 1317–1328, 1994.
- Medwin, H., and N. D. Breitz, Ambient and transient bubble spectral densities in quiescent seas and under spilling breakers, *J. Geophys. Res.*, *94*, 12,751–12,759, 1989.
- Novarini, J. C., R. S. Keiffer, and G. V. Norton, A model for variations in the range and depth dependence of the sound speed and attenuation induced by bubble clouds under wind-driven sea surfaces, *IEEE J. Oceanic Eng.*, *23*, 423–438, 1998.
- Snyder, R. L., L. Smith, and R. M. Kennedy, On the formation of whitecaps by a threshold mechanism. part III: Field experiment and comparison with theory, *J. Phys. Oceanogr.*, *13*, 1505–1518, 1983.
- Thorpe, S. A., On the clouds of bubbles formed by breaking wind waves in deep water, and their role in air-sea gas transfer, *Philos. Trans. R. Soc. London, Ser. A*, *304*, 155–210, 1982.
- Thorpe, S. A., Measurements with an automatically recording inverted echo sounder: ARIES and the bubble clouds, *J. Phys. Oceanogr.*, *16*, 1462–1478, 1986.
- Updegraff, G. E., and V. C. Anderson, Bubble noise and wavelet spills recorded 1 m below the ocean surface, *J. Acoust. Soc. Am.*, *89*, 2264–2279, 1991.
- Wu, J., Bubbles in the near—surface ocean—Their various structures, *J. Phys. Oceanogr.*, *24*, 1955–1965, 1994.
- Wu, J., Concentrations of sea-spray droplets at various wind velocities: Separating productions through bubble bursting and wind tearing, *J. Phys. Oceanogr.*, *30*, 195–200, 2000.

P. M. Kalvoda, Visteon Corporation, 17000 Rotundra Drive, Dearborn, MI 48121, USA. (pkalvoda@visteon.com)

J. Wu, Institute of Hydraulic and Ocean Engineering, National Cheng Kung University, Tainan 701, Taiwan. (jinwu@mail.ncku.edu.tw)

L. Xu, Ocean University of Qingdao, Qingdao 266003, China.